Mechanistic Investigation of the Growth of $Fe_{1-x}Co_xSi$ ($0 \leq x \leq 1$) and $Fe_5(Si_{1-y}Ge_y)_3$ ($0 \leq y \leq 0.33$) Ternary Alloy Nanowires

Jeremy M. Higgins,[†] Penelope Carmichael,[†,‡] Andrew L. Schmitt,[†] Stephen Lee,[†] John P. Degrave,[†] and Song Jin[†,*]

[†]Department of Chemistry, University of Wisconsin—Madison, 1101 University Avenue, Madison, Wisconsin 53706, United States, and [‡]School of Chemistry, University of Bristol, Bristol BS8 1TS, England

ABSTRACT We present the chemical vapor deposition (CVD) reactions of the single source precursor $Fe(SiCl_3)_2(CO)_4$ over Si, Ge, $CoSi_2$/Si, and CoSi/Si substrates to explore the growth and doping processes of silicide nanowires (NWs). Careful investigation of the composition and morphology of the NW products and the intruded silicide films from which they nucleate revealed that the group IV elements (Si, Ge) in the NW products originate from both the precursor and the substrate, while the metal elements incorporated into the NWs (Fe, Co) originate from vapor phase precursor delivery. The use of a Ge growth substrate enabled the successful synthesis of Fe_5Si_2Ge NWs, the first report of a metal silicide—germanide alloy NW. Further, investigation of the pyrolysis of the $CoSiCl_3(CO)_4$ precursor revealed independent delivery of Co and Si species during CVD reactions. This understanding enabled a new, more robust two-precursor synthetic route to $Fe_{1-x}Co_xSi$ alloy NWs using $Fe(SiCl_3)_2(CO)_4$ and $CoCl_2$.

KEYWORDS: nanowire · silicide · germanide · diffusion · single source precursor · chemical vapor deposition

Metal silicide nanowires (NWs)[1] are being pursued for applications in electronics,[2−4] spintronics,[5,6] thermoelectrics,[7−9] and solar energy harvesting.[10] Recent research efforts have realized the successful NW synthesis of more than 20 different metal silicide phases *via* two types of methods:[1] (1) a conversion approach in which silicon NWs are reacted with evaporated metal;[11,12] and (2) single step vapor phase reactions in which vaporous metal and/or silicon sources, such as vaporized elements,[13,14] metal halides,[4,15,16] or silane,[17] are delivered to silicon or metal growth substrates, which often serves as an elemental source for NWs. For example, single source precursor (SSP) chemical vapor deposition (CVD), the pyrolysis of silicon and metal containing molecules over a silicon substrate, has been demonstrated for the successful synthesis of FeSi,[18,19] CoSi,[20] $MnSi_{1.8}$,[8] and doped (or alloyed) $Fe_{1-x}Co_xSi$ NWs.[5] Despite such synthetic success, a clear understanding of how this direct silicide NW growth occurs has remained elusive.[1] Perhaps the most important unanswered questions are (i) the process(es) of precursor species delivery and their roles in NW phase formation and selection and (ii) the origin of anisotropic growth in silicide NWs. Common NW materials,[21] such as Si[22] and ZnO,[23] have simple phase behavior and grow anisotropically *via* the use of a nanoscale catalyst[22] or the manipulation of a screw dislocation.[23−25] In contrast, the synthesis of metal silicide NWs is complicated by the complex phase behaviors of metal−silicon systems,[19] and the NW growth mechanism(s) is yet unidentified, as the telltale signs of catalyst particle tip or axial dislocations have not been observed. A commonly referenced "vapor−solid" mechanism[26,27] is sometimes invoked for silicide NW growth but never accompanied with a sound rationalization for anisotropic growth.

Regardless of the specific synthetic approaches, most silicide NWs are observed to directly grow from films, crystals, or protuberances near the NW−substrate interface. Furthermore, several reports have highlighted the importance of surface silicon oxides[18] or metal oxides[28,29] and crystalline[13,14] or amorphous[30] silicide layers in influencing and controlling NW formation, while no catalyst has ever been observed at the tip of these NWs. More detailed investigation of the NW−substrate interface is clearly necessary. Further, the chemical details of precursor transport, delivery, and reaction that are crucial to understanding the NW phase formation sequence are poorly studied. Control over this material supply could enable a rational synthetic approach to NWs of doped (alloyed) binary

* Address correspondence to jin@chem.wisc.edu.

Received for review January 30, 2011 and accepted February 25, 2011.

Published online March 11, 2011
10.1021/nn200387y

or ternary silicide phases important for technological applications, such as alloyed NWs of semiconducting $Mn(Si_{1-x}Ge_x)_{1.8}$ for thermoelectrics[8,31] and $Fe_{1-x}Co_xSi$ NWs[5] for spintronics.

The purpose of this article is to explore the roles substrate films and precursor decomposition play in the formation and doping of silicide NWs. To fulfill this purpose, we first look to the decades of research in the growth of bulk and thin film metal silicides, which has revealed several fundamentally limiting growth phenomena[32,33] (nucleation, diffusion, and chemical reaction) and given some insight into the nucleation order of bulk metal silicides.[34,35] There is no reason to believe that silicide NW phase formation ought to be governed by rules different from other silicide morphologies. Rather, silicide NWs and other nanomaterials merely present a different set of limiting conditions defined by their nanoscale morphologies, similar to the differences in phase formation observed in bulk and thin film silicide materials.[32] To this end, we studied CVD of the SSP $Fe(SiCl_3)_2(CO)_4$ over silicon, germanium, $CoSi_2$ films on Si, and CoSi films on Si substrates, as summarized in Scheme 1a–d. In that process, we revealed evidence for the mobility of group IV species in the growth substrates and the importance of vapor phase species in determining NW composition. We synthesized $Fe_5(Si_{1-x}Ge_x)_3$ alloy NWs for the first time (Scheme 1b), the first example of a silicide–germanide alloy NW. We further explored the chemistry of SSP decomposition and used this knowledge to develop a new and improved method to produce $Fe_{1-x}Co_x$ Si NWs (Scheme 1e).

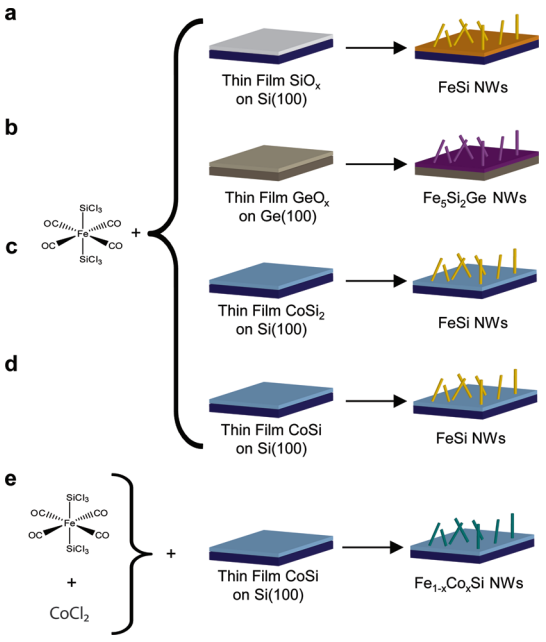

Scheme 1. Chemical synthesis of FeSi, Fe_5Si_2Ge, and $Fe_{1-x}Co_xSi$ alloy NWs using CVD of the single source precursor $Fe(SiCl_3)_2(CO)_4$ and a range of substrates.

RESULTS AND DISCUSSION

Characterization of *In Situ* Grown Silicide Film. We first focus on the relatively well-studied SSP-CVD synthesis of FeSi NWs using $Fe(SiCl_3)_2(CO)_4$ and Si substrates covered with 1–2 nm SiO_x (Scheme 1a), wherein powder X-ray diffraction (PXRD) of as-grown substrates has revealed only iron monosilicide (FeSi).[18] To probe the relationship between surface film and NW nucleation and growth, we carried out a series of standard FeSi NW synthesis experiments on patterned substrates[19] and quenched the reactions at early times. Scanning electron microscopy (SEM) of a 5 min reaction (Figure 1a) confirms that the NWs and film have both already nucleated. While many small islands are visible, NWs are observed to grow only from these film deposits.

To further examine this film, we used FIB milling to expose the substrate cross sections and reveal a number of interesting features (Figure 1b). Below the NW surface, we observe a continuous film with sparse small voids above a heavily voided region. Below the large voids, we see a thin continuous film with a clear interface with the Si substrate. Growth on a patterned substrate reveals that the film intrudes up to 2–3 μm into the initial substrate surface without obvious volume expansion. FeSi is nearly twice as dense as Si (roughly 88 and 50 atoms per nm^3, respectively),[36] so perhaps significant volume expansion is not expected for the incorporation of Fe into Si. Voids such as those observed in our samples are often seen in diffusion-based reactions systems where one component diffuses more quickly than the other and are termed Kirkendall voids.[37,38] The presence of voids closer to the Si surface implies that Si is the dominant diffusing species in this silicide film as we would expect in FeSi.[39]

To further analyze the morphology of this intruded silicide film, cross-sectional transmission electron microscopy (CSTEM) samples were prepared by combined microcleavage[40] and FIB polishing methods.[41] Special attention was paid during fabrication to maintain the integrity of the silicide film by depositing a protective Pt film on the surface. Select area electron diffraction (SAED) (Figure 1g) from this intruded silicide film was characteristic of a polycrystalline film. Rotational average and analysis on the original SAED pattern using the DiffTools package[42] (Gatan Micrograph Suite) showed that only the FeSi phase is present in the intruded silicide film. FeSi is the phase predicted to form first between Fe and Si thin films according to the "first-phase rule".[34,35] TEM micrographs of this intruded polycrystalline silicide film (Figure 1c–f) reveal that the size of FeSi crystallites above and below the void-heavy region is different (Figure 1d,f). The intruded silicide film below the voids shows a clear angular interface with the silicon substrate and appears to be composed of nearly columnar grains on the order of 200 nm in size. The grains of the silicide film above the voids are smaller and more densely

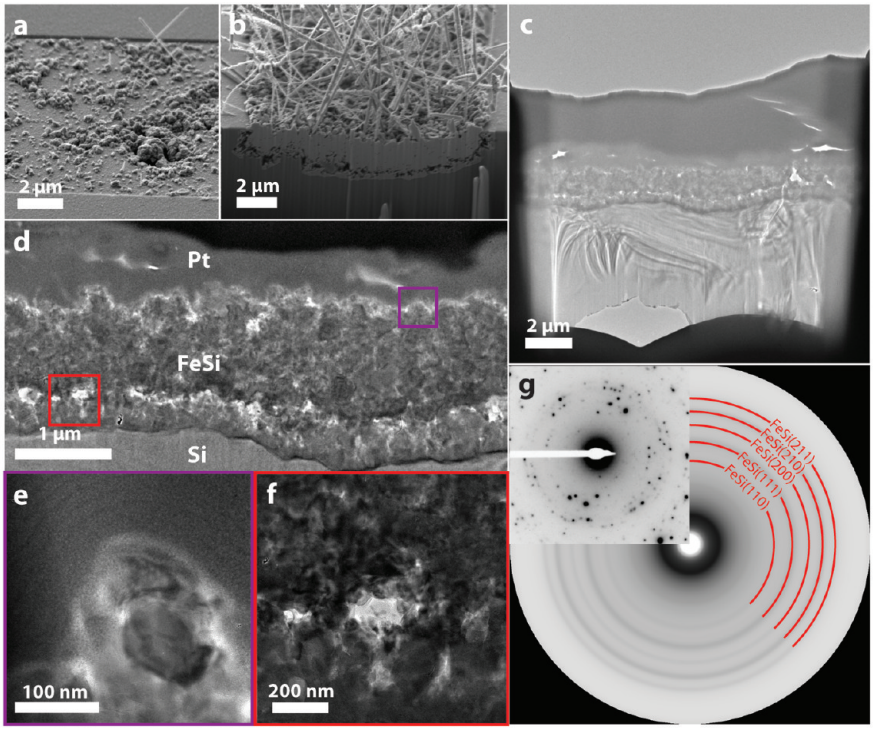

Figure 1. Characterization of the intruded FeSi film from the SSP-CVD synthesis of the FeSi NWs. (a) SEM image of 5 min reaction on a patterned substrate revealing simultaneous formation of film and NWs growing from the film. (b) SEM image of a focused ion beam cross section of a standard patterned FeSi NW growth substrate. (c) TEM images of a cross-sectional TEM FeSi NW growth substrate with images highlighting the (d) various layers, (e) surface structures, and (f) void space region. (g) SAED of the intruded silicide film and rotational average of the SAED showing the expected FeSi ring positions.

packed with sizes ranging from 20 to 200 nm. This morphology extends to the substrate surface where protuberances containing small crystallites are observed (Figure 1e). These protrusions have the same size as the diameters of the NWs that grow from such substrates and are likely the bases or nucleation sites of NWs, though no NW was successfully captured due simply to the low probability of catching a NW perfectly oriented in a film the thickness of the CSTEM samples. A similar analysis was completed on a CoSi NW growth substrate and revealed a similar two-region, heavily voided, polycrystalline morphology (Figure S1 in Supporting Information).

These observations show that the CVD reaction of $Fe(SiCl_3)_2(CO)_4$ over a 1−2 nm SiO_x/Si substrate resulted in a complex FeSi NW/intruded silicide/Si heterostructure, and the formation of this underlying FeSi film appears to be an important prerequisite for the subsequent growth of FeSi NWs. The small FeSi crystallites in the upper region of the silicide film might help facilitate the nucleation and growth of FeSi NWs (perhaps the grain boundary between the FeSi NW base and the growth surface could be a potential growth interface for VSS or some similar growth mechanism[43]), though the exact mechanism for anisotropic growth remains unclear. The Kirkendall voids within the silicide film strongly suggest that Si is mobile and likely being incorporated into the NW products through diffusion from the underlying substrate. The observation of etch pits on as-grown Si substrate surfaces by other researchers[13,14] has implied that Si supply to NWs may occur through surface-mediated processes. Our observation highlights the mobility of Si in the growth substrate *via* bulk diffusion but does not, of course, rule out the delivery of Si species from the substrate through etching and formation of $SiCl_4$ or other gaseous Si species or the mobility of Si on the substrate *via* surface diffusion. On the basis of these results, further investigation of diffusion of materials from different substrates became obvious.

Synthesis and Characterization of $Fe_5(Si_{1-x}Ge_x)_3$ Alloy NWs on Ge Substrates. We carried out the same CVD reactions of $Fe(SiCl_3)_2(CO)_4$ over a Ge substrate (Scheme 1b) instead of 1−2 nm SiO_x/Si(100) substrates and looked for the evidence for Ge incorporation in the NW products. This approach allows us to ask whether the Si found in silicide NWs originates from the substrate or the SSP during the SSP-CVD growth of NWs. Oxide films were grown on these Ge growth substrate surfaces by subjecting them to elevated temperature (400 °C) in air; an oxidation time of 4 min resulted in the most dense and longest NWs.

The resulting sample morphology (Figure 2a) consists of a rough film, micrometer scale crystals, and moderately dense NWs roughly 10 μm in length with diameters broadly ranging from 50 to 500 nm. PXRD was

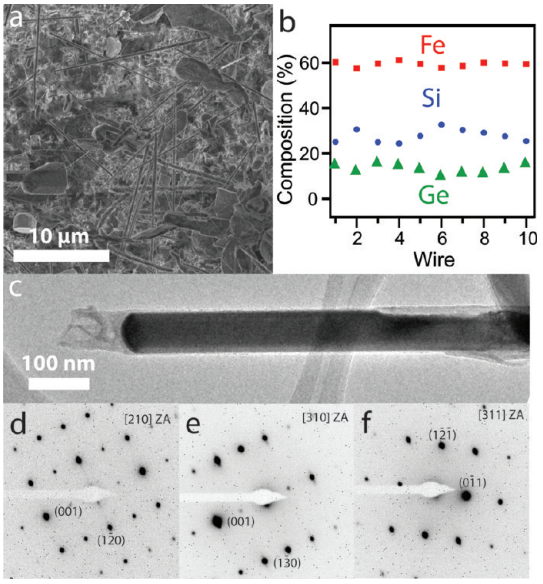

Figure 2. Growth of $Fe_5(Si_{1-x}Ge_x)_3$ NWs on Ge substrates. (a) SEM image of as-grown substrate revealing the NWs and other observed morphologies. (b) Composition of 10 NWs identified *via* EDX. (c) TEM image of a NW analyzed *via* SAED. (d−f) SAED patterns taken from the same NW, which are in excellent agreement with the [120], [130], and [131] zone axes of the Fe_5Si_3 structure type.

completed on the as-grown substrate, but no obvious match has been identified (Figure S2 in Supporting Information). Within the SEM, it was clear that the NWs had a coating, identified as silicon oxide by EDX (Figure S3), which manifested most thickly at NW tips. NWs were transferred to lacey carbon coated Cu TEM grids for compositional and crystallographic analysis. EDX analysis of 10 NWs that had been treated with buffered HF to remove surface oxide revealed an average atomic composition of 59% Fe, 28% Si, and 13% Ge (Figure 2b). Each NW was scanned twice, at least a micrometer apart, revealing composition variations of less than 2% for any given element. While the Fe composition varied very little between NWs, the ratio of Si/Ge fluctuated from roughly 3:1 to 2:1. Variations in Ge concentration tracked closely with those in Si concentration, pointing to substitutional alloying in the NWs. The Fe−Ge and Fe−Si phase diagrams near this composition are quite rich with many related hexagonal phases requiring careful diffraction analysis to identify.

TEM was completed on a NW sample which still had the SiO_x coating on their surface (Figure 2c). As shown in Figure 2d−f for one representative example, multiple SAED patterns were taken from one NW with special care taken to record the angles between observed zone axes. The three patterns were consistent with Fe_5Si_3 (space group $P6_3/mcm$, $D8_8$ structure type) observed in the Fe−Si phase diagram. The lattice parameters were measured to be $a = 6.9 \pm 0.1$ Å and $c = 4.8 \pm 0.1$ Å, slightly larger than the lattice parameters reported for the pure Fe_5Si_3 phase ($a = 6.7416(6)$ Å, $c = 4.7079(6)$ Å).[44] The measured angles between the observed zone axes, [120] ∠ [130] = 11.6°, [120] ∠ [131] = 18.9°, and [130] ∠ [131] = 15.5°, were consistent within measurement error with the Fe_5Si_3 structure type (expected angles between Fe_5Si_3 crystallographic directions [120] ∠ [130] = 10.89°, [120] ∠ [131] = 18.29°, and [130] ∠ [131] = 14.79°). NWs have a surface amorphous coating of 10−15 nm thick on the NW surfaces, and the morphology of the SiO_x at the NWs' ends is suggestive of a tube, which might be relevant to the growth of these NWs.

EDX and SAED analysis taken together, it is clear that the decomposition of the SSP $Fe(SiCl_3)_2(CO)_4$ over an oxidized Ge substrate resulted in the incorporation of Ge in the NW product synthesized, the NW phase changed from B20 FeSi to the more metal-rich Fe_5Si_3 structure type, and that the NWs have the approximate composition of Fe_5Si_2Ge. Clearly, the Si and Ge in the silicide−germanide alloy NWs originate from both the SSP and the substrate, as these are the only Si and Ge sources in the reaction, respectively. It is interesting that the more metal-rich phase is observed in these NWs. Fe_5Si_3 and $Fe_{1.3}Ge$ NWs were recently reported during the CVD reaction of FeI_2 with a sapphire substrate placed on top of Si or Ge sources.[45,46] The authors explain the production of the more metal-rich silicide (germanide) NW phases as arising due to decreased partial pressure of the intermediate SiI_4 (GeI_4) in the vicinity of the sapphire substrate. For our case, the supply of Si from the SSP to the Ge substrate is the same as in the reaction with a Si substrate, so our observation of a metal-rich $Fe_5(Si_{1-x}Ge_x)_3$ alloy phase implies that the group IV element supply is somehow limited by decreased diffusion from the Ge substrate and/or by slower production of a $GeCl_4$ intermediate. Regardless, this is the first report of substitutional alloying of Ge in a metal silicide NW, opening up a whole new class of metal silicide−germanide alloy NW materials for study.

Reaction of $Fe(SiCl_3)_2(CO)_4$ over $CoSi_2$ Film on Silicon Substrates. While the $Fe_5(Si_{1-x}Ge_x)_3$ alloy NW formation is an exciting result, there is also interest in controllable synthesis of $Fe_{1-x}Co_xSi$ NWs and other metal alloyed silicide NWs for spintronics studies. Recent reports of $Fe_{1-x}Co_xSi$ NW synthesis[5,6] established that alloy formation was feasible using two different *vapor phase* metal precursors, but neither report was able to demonstrate a controllable process allowing one to "dial-in" a Fe/Co ratio in the silicide NWs. Further, Ni and Fe were successfully incorporated into $TaSi_2$ NWs with substitution as high as 25%, that is, $Ta_{0.75}Fe_{0.25}Si_2$, by synthesizing $TaSi_2$ NWs on $FeSi_2$ and $NiSi_2$ films,[13,14] but demonstrable control over this ternary alloy formation was also lacking. On the basis of the results so far, it seemed reasonable to attempt to employ a metal silicide film as the growth substrates and source of a new metal to potentially enable the experimental study of metal incorporation into silicide NWs from the substrates.

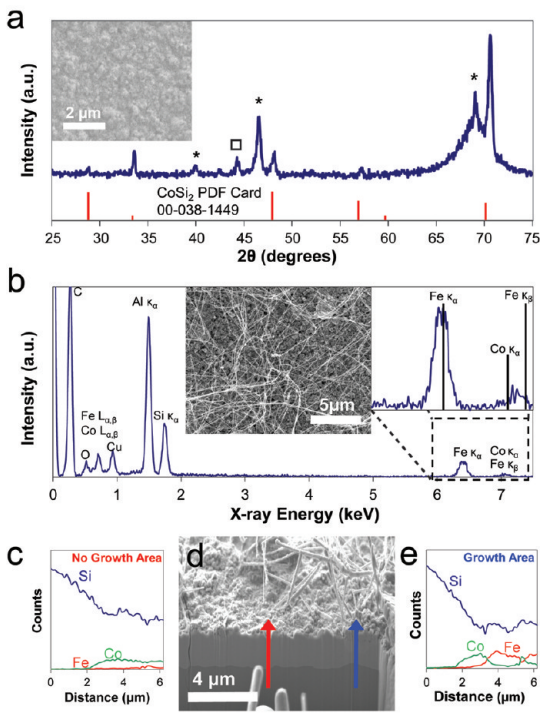

Figure 3. CVD of $Fe(SiCl_3)_2(CO)_4$ onto $CoSi_2$/Si(100) thin film substrate, leading to the growth of pure FeSi NWs. (a) PXRD of the substrate before growth along with the standard peaks for $CoSi_2$. Note that the intensity of the standard peaks is displayed logarithmically to emphasize some lower intensity peaks. Starred and squared peaks arise from the underlying Si substrate and remaining Co metal, respectively. Inset is an SEM of the substrate before growth. (b) EDX obtained from NWs produced in the reaction revealing the lack of Co incorporation. Insets show NWs on the as-grown substrate and an expanded view of the Fe and Co K edges. (c−e) EDX line scans taken from an FIB cross-section sample reveal the lack of mixing in iron and cobalt silicide films and show that NWs grow only from iron silicide regions.

The formation of cobalt silicide thin films on silicon wafers by solid state reaction is well-developed, as $CoSi_2$ is a common material in CMOS technology.[33,47] We prepared $CoSi_2$/Si substrates by evaporating Co onto the surface of freshly HF-treated substrate and annealing at elevated temperature and confirmed that the films are $CoSi_2$ with PXRD and SEM (Figure 3a and inset). Dense and high-quality NWs (Figure 3b inset) can be reproducibly grown by CVD of $Fe(SiCl_3)_2(CO)_4$ over these $CoSi_2$/Si substrates following the standard FeSi NW growth procedure (Scheme 1c). While NWs were observed when the surface was intentionally oxidized, the densest NW samples were obtained when synthesized on freshly HF-etched substrates (Figure 3b inset). Interestingly, EDX examination of these NWs showed that they contain only Fe and Si, in a ratio of 1:1 (Figure 3b).

To investigate why Co was not incorporated into these NWs, we prepared FIB cross sections of as-grown substrates. Two different regions of the silicide film are clearly differentiable in the cross-sectional SEM images (Figure 3d). EDX line scans reveal no significant mixing of iron and cobalt in the metal silicide films, that is, a spotty iron silicide film, presumably FeSi, is observed to form on top of the original $CoSi_2$ film. NWs are only observed to grow from regions capped with iron silicide film (Figure 3c−e).

These results show that, while $CoSi_2$ film can facilitate the growth of FeSi NWs, the NWs only nucleate and grow from the iron silicide film produced *in situ* on top of the $CoSi_2$ substrate, and Co from the $CoSi_2$ film does not find its way into either the *in situ* generated silicide film or the silicide NWs. In most silicon-rich silicides, Si is the dominant diffusing species,[48] but at relatively high temperature, the diffusivities of Co and Si in $CoSi_2$ are quite similar.[49] Specifically, at the NW growth temperature, one would expect diffusion lengths ($L = (Dt)^{1/2}$) of 0.59 and 3.0 nm in 1 s for Co and Si, respectively. The lack of Co in the resulting FeSi film and NWs seems to rule out the incorporation of metal from the substrate; therefore, metal incorporation must occur *via* either a surface-mediated diffusion process or a vapor phase reaction. One could, however, argue that the $CoSi_2$ film we used in this reaction is different from the silicide film that normally grows *in situ* alongside FeSi and CoSi NWs in phase or morphology and potentially causes different growth and doping behavior.

Reaction of $Fe(SiCl_3)_2(CO)_4$ over CoSi Films Grown Using SSP-CVD. To rule out the possibility of a difference between the silicide films *in situ* grown *via* CVD and those generated *ex situ*, we further used an *in situ* deposited CoSi film as a substrate for FeSi NW growth to investigate if Co will be incorporated into the FeSi NW product. We prepared the CoSi film by following previously reported CoSi NW synthesis procedures[20] and removing the NWs by sonication. PXRD of these films revealed peaks from both CoSi and $CoSi_2$, in agreement with previously published results (Figure 4a), although the previous report does not explicitly identify the $CoSi_2$ peaks.[20] These cobalt silicide films have a very similar morphology to the FeSi silicide film (Figure S1 in Supporting Information). When these SSP-CoSi/Si substrates were freshly HF-etched and used as the growth substrate for the FeSi SSP-CVD reaction (Scheme 1d), dense and smooth NWs were obtained (Figure 4b inset). Interestingly, EDX of these NWs revealed Fe/Si ratios on the order of 1:1 and again no incorporation of Co (Figure 4b), which is effectively identical to that observed using a $CoSi_2$ substrate.

Why can NWs of the same FeSi phase be obtained when $Fe(SiCl_3)_2(CO)_4$ is pyrolyzed over oxidized Si, $CoSi_2$ and CoSi surfaces with no Co incorporation into the product? We can use the interplay of diffusion and vapor phase reactant supply to explain these results. In each case, FeSi NWs grow from a FeSi layer first formed, simplifying material supply analysis.

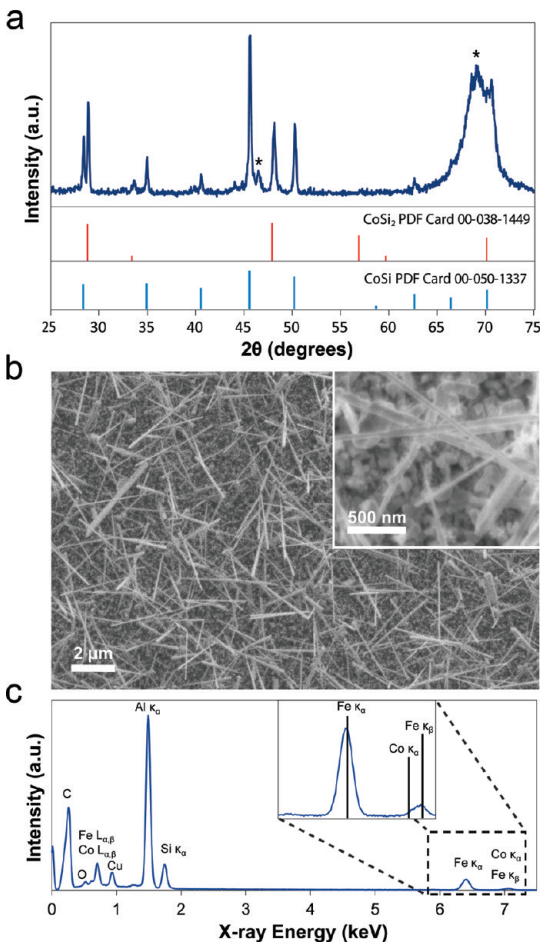

Figure 4. CVD of $Fe(SiCl_3)_2(CO)_4$ onto SSP-CoSi/Si(100) thin film substrate leading to the growth of FeSi NWs. (a) PXRD of the substrate before growth along with the standard peaks for CoSi and $CoSi_2$. Note that the intensity of the standard peaks is displayed logarithmically to emphasize the weak peaks. Starred peaks arise from the Si substrate. (b) SEM of the NWs on the as-grown substrates. (c) EDX obtained from NWs produced in the reaction revealing the lack of Co incorporation. Inset shows an expanded view of the Fe and Co K edges.

In principle, metal could be supplied to a growing NW by either a vapor phase precursor or diffusion through FeSi layers or surface diffusion over FeSi layers. The bulk and surface diffusion of Co and Fe in FeSi should be quite similar,[39,49,50] so the absence of Co in the NW products implies that metal is supplied much faster by the vapor phase precursor than by diffusion from the substrate. In contrast, the results presented above on the formation of Fe_5Si_2Ge NWs using Ge substrate reveal that Si is likely contributed by both the substrate and the vapor phase precursor. However, the rate of material supplied by the substrate and SSP should be similar whether an oxidized Si, $CoSi_2$/Si, or CoSi/Si substrate is used, explaining why the same NW phase is obtained. The observation that the NWs only grew from FeSi layers means that a silicide substrate, like an oxidized silicon substrate, merely enables appropriate deposition of FeSi to seed NW growth. FeSi NW samples grown using $CoSi_2$/Si and CoSi/Si substrates were more dense and reproducible than those obtained on oxidized Si, perhaps merely because of the rough and reactive polycrystalline film. Using a silicide film as a substrate is the more effective and reproducible method to "seed" FeSi NW growth and will be used again later for alloy NW growth.

On the basis of the results of reactions of $Fe(SiCl_3)_2(CO)_4$ with oxidized Si, oxidized Ge, $CoSi_2$/Si, and CoSi/Si substrates to produce FeSi and $Fe_5(Si_{1-x}Ge_x)_3$ NWs, we have inferred that incorporation of metals into the final NW product appears to be from vapor phase species with slow diffusion limiting delivery from the substrate while group IV elements can originate from either an intentionally introduced vapor phase species or from the substrate. This complicated interplay of material supply sources, including vapor phase precursors, substrate surface diffusion, and substrate volume diffusion, is likely important for defining the phase of the NW product. The recent reports of metal-rich silicide NWs (Fe_5Si_3, Co_3Si, and Co_2Si) obtained from the CVD reactions of metal halides over sapphire substrates placed on top of Si substrates, in which the authors postulate that halide decomposition results in vapor phase $SiCl_x$,[51] highlight that the chemical details of vapor phase species and their reactions with substrates are important factors in material delivery and NW phase control.

Decomposition Behavior of $CoSiCl_3(CO)_4$. Our results so far indicate that SSPs give rise to much of the silicon and all of the metal incorporated into the silicide NWs. However, the details of SSP molecule thermal decomposition and the reactivity of their pyrolytic byproducts are poorly studied. A better understanding of the chemistry in these systems would enable a more rational approach to silicide NW phase control and doping. The standard NW reaction procedure is always accomplished inside a hot-wall CVD reactor that allows SSP molecules to react well before they reach the growth substrate, as indicated by deposits consistently observed in various regions on the inner walls of the reactor. For pyrolysis of $CoSiCl_3(CO)_4$, a silvery and metallic deposit is seen in the upstream portion of the reaction tube close to the furnace entrance, while the downstream of the reaction tube has a blue deposit just outside of the furnace, which becomes purple and then pink upon exposure to air, and a dull, black deposit further downstream. PXRD and EDX scans of the reaction deposits were taken to determine the identity of the compounds present.

In order to prepare samples for PXRD, we carried out a standard CoSi CVD reaction using a large amount of $CoSiCl_3(CO)_4$ (500 mg) in the absence of any substrate and acquired deposits with typical appearance. The reactor tube was carefully broken apart and the deposits scraped off and analyzed. The silvery material

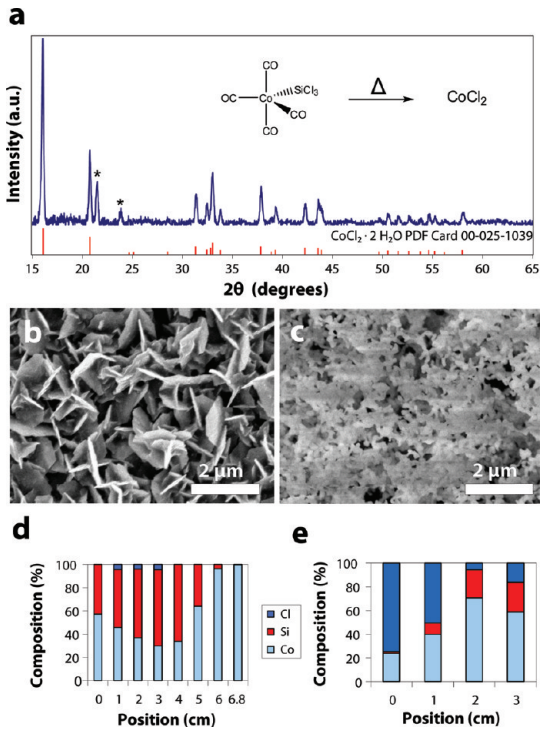

Figure 5. Analysis of the decomposition products of Co(SiCl$_3$)(CO)$_4$. (a) PXRD of downstream deposits identified as CoCl$_2$·2H$_2$O. Starred peaks arise from the grease used in sample preparation. SEM images of material deposited onto copper foils on the (b) upstream and (c) downstream portions of the CVD reactor. Elemental compositions of the deposits collected on copper foils placed in the (d) upstream and (e) downstream portions of the CVD reactor.

deposited upstream was not easily obtained for XRD analysis, but the pink and black deposits observed on the downstream portion of the reaction tube were identified by PXRD as partially hydrated $CoCl_2$ (Figure 5a) and Co_2Si (Figure S4 in Supporting Information), respectively. To obtain additional information, we used EDX to analyze the elemental composition (Figure 5d,e) of the deposits collected onto two pieces of copper foil placed in the CVD reactor, which have similar appearance to those normally seen on the walls of the reactor's quartz tube after a standard CoSi NW synthesis. The deposits from the upstream foil consist mostly of Co and Si and gradually become more metal-rich as higher temperatures in the furnace are reached. SEM images (Figure 5b,c) of the points analyzed reveal a morphological change from a rough polycrystalline film to microplates. In the downstream deposits, chlorine is far more prevalent, Si is present to a much smaller degree, and the transition between the cobalt chloride and cobalt silicide observed in PXRD analysis is clear.

These analyses showed that well before the precursor reaches the substrate significant decomposition has occurred. The presence of Co- and Si-rich deposits in the upstream region of the reactor points to early decomposition of the SSP into separate vapor phase Co and Si species. This is further backed up by the presence of $CoCl_2$ at the downstream of the reactor. One premise of SSP-CVD is the controlled delivery of single precursor molecules having metal and silicon in a set ratio to a growth substrate. These studies suggest that in the case of Co(SiCl$_3$)(CO)$_4$ separate species are delivered to the growth substrate surface. However, the SSP approach, having already been successfully used to synthesize NWs of a number of metal silicide phases,[1] can still provide several benefits. For example, SSPs vaporize or sublime at temperatures significantly lower than the halides and metallic species used in other silicide synthetic methods, and they provide a *reproducible* delivery of a fixed ratio of precursor species.

Improved Synthesis of Alloyed Fe$_{1-x}$Co$_x$Si NWs by Combining SSP and CoCl$_2$. To date, successful CVD synthesis of Fe$_{1-x}$Co$_x$Si NWs has been accomplished using mixtures of Fe(SiCl$_3$)$_2$(CO)$_4$ with Co(SiCl$_3$)(CO)$_4$[5] or FeI$_2$ with CoI$_2$.[6] In either case, the mixtures of precursors with different melting points, and thus vapor pressures, were subjected to the same sublimation temperature, typically just over 100 °C for SSP molecules[52] and near or above 500 °C for the halides. Similar sublimation or vaporization temperatures of the precursor mixtures resulted in the inability to control the vapor pressure of these species independently and thus poor control over composition. The mixed halide precursor did not allow the synthesis of broad Fe$_{1-x}$Co$_x$Si alloy compositions beyond $x = 0.10$. The mixed SSP approach, while capable of yielding many alloy compositions, is also hard to reproduce. The improved understanding of the SSP decomposition allowed us to design a new scheme for synthesizing Fe$_{1-x}$Co$_x$Si NWs with better control using one SSP and one halide as precursors.

CVD reactions of Fe(SiCl$_3$)$_2$(CO)$_4$ and $CoCl_2$ loaded into separate alumina boats onto freshly HF-etched SSP-CoSi/Si (Scheme 1e and Figure 6a) resulted in dense NWs roughly 50 to 100 nm in diameter and 10 μm or more in length with quite smooth surfaces (Figure 6c). In all cases, we followed a modified standard reaction procedure changing only the position of the $CoCl_2$ boat. The Co composition in the NW products most critically depends on the precise position of the $CoCl_2$ precursor in the CVD reactor. Also the most reproducible results were obtained when the $CoCl_2$ in the boat was loaded in as tight a pile as possible, covering approximately 3 mm, due to the large thermal gradient at the boat's location in the furnace. We report on two successful doping reactions with the alumina boat centered at $d = 6.5$ and 7.5 cm downstream from the furnace edge (Figure 6a). EDX analysis was completed for three different NWs in each sample (Figure 6b). For the sample positioned at 6.5 cm, a small shoulder on the low energy side of the Fe Kα peak can be observed, corresponding to the position of the Co Kα peak while the 7.5 cm sample shows clear signals from both Fe K*a* and Co K*a* peaks. Quantitative

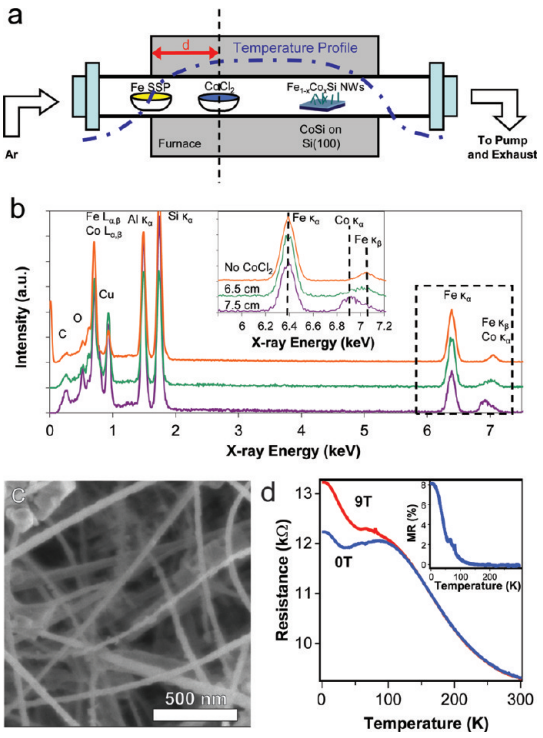

Figure 6. Synthesis of $Fe_{1-x}Co_xSi$ NWs *via* CVD of $Fe(SiCl_3)_2(CO)_4$ and $CoCl_2$ onto SSP-CoSi/Si(100) substrates. (a) Schematic diagram detailing the important growth parameters for this CVD process. (b) EDX spectra for syntheses using no $CoCl_2$ (top, orange), a $CoCl_2$ boat centered at 6.5 cm (center, green), and a $CoCl_2$ boat centered at 7.5 cm (bottom, violet). Inset highlights the Fe and Co K edges and the increase in the Co Kα edge from top to bottom curves. (c) SEM of $Fe_{1-x}Co_xSi$ NWs synthesized using this scheme. (d) Zero field cooled *R vs T* trace of an $Fe_{1-x}Co_xSi$ NW device at 0 and 9 T revealing the positive transverse magnetoresistance characteristic of $Fe_{1-x}Co_xSi$. Inset shows magnetoresistance (MR) as a function of *T*.

analysis revealed Fe/Co/Si ratios of 53:2:45 and 35:15:50 for the 6.5 and 7.5 cm samples, respectively, giving roughly $Fe_{0.96}Co_{0.04}Si$ and $Fe_{0.70}Co_{0.30}Si$. Reactions carried out with the $CoCl_2$ boat centered at 6 cm gave rise to FeSi NWs with no Co incorporation, and reactions carried out with the $CoCl_2$ boat centered at 8 cm gave rise to Co_2Si NWs. These metal-rich Co_2Si NWs, some of which even showed Fe incorporation, were sometimes observed as a byproduct of this reaction and have been previously seen when using a mixture of $Fe(SiCl_3)_2(CO)_4$ and $CoSiCl_3(CO)_4$ as precursors for $Fe_{1-x}Co_xSi$ NW synthesis.[5]

We further fabricated NW devices from the $Fe_{0.70}Co_{0.30}Si$ NW sample using standard lithographic methods and measured their *R*−*T* properties (Figure 6d) to verify the successful substitutional doping with this new synthesis. The zero field cooled resistance as a function of temperature at 0 and 9 T and magnetoresistance (MR = $[R(9T) - R(0T)]/R(0T) \times 100\%$) as a function of temperature (Figure 6e and inset) reveals the characteristic shape and qualitative behavior common to $Fe_{1-x}Co_xSi$ crystals[5,53] with a peak MR near 8% under a 9 T field at 2 K. This magnetotransport characterization confirms the successful synthesis of NWs of the substitutional alloy $Fe_{1-x}Co_xSi$ using the new two precursor approach.

CONCLUSION

We have described careful exploration of metal silicide NW formation processes using SSP-CVD growth of silicide NWs on Si, Ge, $CoSi_2$/Si, and CoSi/Si substrates. These results have clarified the origins of the elements incorporated into NW products, highlighted the importance of precursor chemistry and diffusion in this process, and enabled more controllable and robust production of alloy NWs. Specifically, we revealed that group IV (Si, Ge) elements in the substrate are clearly mobile and the Si (Ge) element in the NW products originates from both the substrate and the vapor phase precursor. This allowed the successful synthesis of Fe_5Si_2Ge NWs, the first metal silicide−germanide alloy NW species. In contrast, our attempts to incorporate metal using silicide substrates were unsuccessful but revealed that vapor phase delivery of metal occurs far more quickly than metal diffusion from the substrates. We have also begun the broader exploration of precursor chemistry by investigating the decomposition of SSP $CoSiCl_3(CO)_4$. We observed signs of independent Co and Si transport to growth substrates with Co transport occurring through the intermediate $CoCl_2$. This realization allowed us to develop a new two-source CVD process for the synthesis of $Fe_{1-x}Co_xSi$ NWs with more control than previous approaches using $Fe(SiCl_3)_2(CO)_4$ and $CoCl_2$ as independently adjustable material sources. This capability to independently introduce different materials should enable additional mechanistic investigation, for example, the determination of tip or base growth in silicide NWs.

Although our exploration has focused on silicide NW growth using SSP-CVD, the results and understanding should have general implications to silicide NW growth using other synthetic strategies. Fundamentally, the processes that lead to the formation of metal silicide NWs (or other intermetallic NWs in general), reaction of precursors in the gas phase or with surfaces, transport of material *via* diffusion, and nucleation and growth of 1D nanostructures, should be universal among various synthetic strategies with the apparent differences originating from the details of chemical processes. The results presented herein bring new understanding to the nucleation of silicide NWs, elucidate the impact of the growth substrate on material delivery, and enhance our understanding of the importance of precursor chemistry on NW growth. This improved knowledge has enabled more robust NW syntheses and the observation of a new NW phase. Many advances have been made in developing the current catalogue of silicide NWs, but further work on rationally controlling

NW phase, composition, and nucleation in bottom-up synthetic approaches will require more thoughtful and pointed experiments. This is the only way that the mysteries of silicide NW growth can be solved.

METHODS

Standard Silicide NW Growth Procedure. All NW syntheses were carried out in a home-built chemical vapor deposition (CVD) reactor in a Lindberg/Blue M tube furnace, as described previously.[18] Various growth substrates were cleaned and coated with a thin film (Scheme 1), the identity and morphology of which was dependent upon the experimental goals, before being placed in the hot zone of the reaction tube, 1 in. upstream of the furnace center. One hundred milligrams of $Fe(SiCl_3)_2(CO)_4$ SSP was placed in a 3 cm long alumina boat and loaded into the vacuum system outside the furnace. The system was evacuated and flushed with argon at a flow rate of 150 sccm and a pressure of 200 Torr. The system was brought to a temperature of 750 °C, and the precursor boats were placed with 0.75 cm of the boat inside the furnace housing (~150 °C) using magnetic stir bars. Once all of the SSP had been consumed (approximately 20−25 min), reactions were terminated.

Synthesis of $Fe_{1-x}Co_xSi$ NWs Using $Fe(SiCl_3)_2(CO)_4$ and $CoCl_2$. An alumina boat with 40 mg of $CoCl_2$ was loaded into the CVD reactor along with an alumina boat filled with 100 mg of $Fe(SiCl_3)_2(CO)_4$ SSP and a magnetic stir bar fitted with a hook made from tungsten wire for a reaction following the standard silicide NW reaction condition. Once the correct temperature was reached, the boats were placed at predetermined positions with the aid of the stir bar tool. The Fe SSP boat was placed as in a standard FeSi NW reaction, while the $CoCl_2$ boat was positioned inside the furnace between $d = 6.0$ and 8.0 cm from the edge of the furnace housing (Figure 6a).

Preparation of Various Cobalt Silicide Thin Films as Nanowire Growth Substrates. *Preparation of $CoSi_2$ Film via Solid Phase Reaction.* Si(100) substrates (25 × 25 × 0.1 mm^3) were sonicated in deionized water, rinsed with deionized water, ethanol, and 2-propanol, dried with N_2 flow, and etched with buffered HF (Buffered HF Improved, Transene Inc.) for 10 s before it was loaded quickly into a metal evaporator (Angstrom Engineering) and evacuated to a base pressure of 2×10^{-6} Torr. Co (99.9999%, Sigma-Aldrich) was e-beam evaporated onto substrates at a rate of 1−2 Å/s to a 500 nm thickness. These Co-covered substrates were annealed at a temperature of 750 °C for 16 h in a CVD furnace under Ar atmosphere (flow rate of 100 sccm and pressure of 760 Torr). PXRD was performed using a STOE powder X-ray diffractometer to confirm the phase formed.

Formation of CoSi Thin Films via SSP-CVD. Si(100) substrates (25 × 25 × 0.1 mm^3) were cleaned and etched as above, but additionally subjected to a 10 min treatment in a metal etch solution (1:1:5 v/v of concentrated HCl/30% H_2O_2/deionized water) at 70 °C to produce a thin (1−2 nm) silicon oxide layer following previously reported procedures.[20] $Co(SiCl_3)(CO)_4$ SSP was placed in an alumina boat 0.5 cm away from the furnace entrance, evaporated, and carried into the reactor with a 150 sccm Ar flow under a pressure of 200 Torr. Reactions were carried out at a temperature of 750 °C for 15 min. Any NWs obtained on these substrates were removed using ultrasonication, leaving a CoSi-film-covered silicon substrate. PXRD was performed using a STOE powder X-ray diffractometer to confirm the phase formed.

Preparation of Cross-Section SEM and TEM Samples. *Focused Ion Beam (FIB) Milling of Growth Substrates.* FIB milling of sample substrates enabled cross-sectional SEM and EDS inspection of the NW growth substrates. A Zeiss Crossbeam SEM-FIB workstation equipped with a FE-SEM electron column, a Ga-ion column, and a SiLi EDS detector was used for this sample preparation and analysis. The substrates were oriented normal to the Ga beam to facilitate milling. The use of various apertures allowed variation of the 30 kV Ga beam current; specifically, sequential use of coarse (2 nA), medium (500 pA), and fine (50 pA) milling currents diminished the impact of milling-induced artifacts on the analysis.

Preparation of CSTEM Samples. FeSi NWs were grown on a thin Si substrate (1 cm × 1 cm × 90 μm) using the previously reported procedure.[18] As-grown substrates were then cut into small wedges using a modified microcleavage technique[40] and glued to Cu support rings (South Bay Technologies) using silver epoxy (South Bay Technologies). These samples were roughly aligned on a Fortress TEM sample holder (South Bay Technologies) and loaded into the FIB system. The samples were imaged *via* SEM to locate a region of the sample surface with an appropriately high density of NWs. Successive electron-beam-induced deposition (~1 μm) and ion-beam-induced Pt deposition (~2 μm) were carried out to protect the samples surface, and then FIB milling was carried out to produce sample with a thickness on the order of 100 nm. Various apertures and voltages were used to control the Ga-ion beam current giving rise to coarse mill (30 kV, 8 nA), medium mill (30 kV, 2 nA), fine mill (30 kV 100 pA), coarse polish (30 kV, 50 pA), and fine polish (5 kV, 100 pA) milling sequences. The thickness of the milled sample was monitored *via* SEM imaging using a secondary electron detector and various SEM imaging voltages.

Acknowledgment. We thank the NSF (CBET-1048625), University of Wisconsin—Madison graduate school, the Sloan Research Fellowship, and Research Corporation Cottrell Scholar Award for support. P.C. thanks the University of Bristol for support.

Supporting Information Available: Cross-sectional TEM of CoSi NW growth substrates, PXRD of the Ge substrate after the CVD of $Fe(SiCl_3)_2(CO)_4$, EDX analysis of the surface coating on Fe_5Si_2Ge NWs, and PXRD of $CoSiCl_3(CO)_4$ CVD byproducts. This material is available free of charge *via* the Internet at http://pubs.acs.org.

REFERENCES AND NOTES

1. Schmitt, A. L.; Higgins, J. M.; Szczech, J. R.; Jin, S. Synthesis and Applications of Metal Silicide Nanowires. *J. Mater. Chem.* **2010,** *20*, 223–235.
2. Liao, L.; Lin, Y.-C.; Bao, M.; Cheng, R.; Bai, J.; Liu, Y.; Qu, Y.; Wang, K. L.; Huang, Y.; Duan, X. High-Speed Graphene Transistors with a Self-Aligned Nanowire Gate. *Nature* **2010,** *467*, 305–308.
3. Song, Y.; Schmitt, A. L.; Jin, S. Ultralong Single-Crystal Metallic Ni_2Si Nanowires with Low Resistivity. *Nano Lett.* **2007,** *7*, 965–969.
4. Song, Y.; Jin, S. Synthesis and Properties of Single-Crystal β_3-Ni_3Si Nanowires. *Appl. Phys. Lett.* **2007,** *90*, 173122/1–173122/3.
5. Schmitt, A. L.; Higgins, J. M.; Jin, S. Chemical Synthesis and Magnetotransport of Magnetic Semiconducting $Fe_{1-x}Co_x$-Si Alloy Nanowires. *Nano Lett.* **2008,** *8*, 810–815.
6. In, J.; Varadwaj, K. S. K.; Seo, K.; Lee, S.; Jo, Y.; Jung, M.-H.; Kim, J.; Kim, B. Single-Crystalline Ferromagnetic $Fe_{1-x}Co_xSi$ Nanowires. *J. Phys. Chem. C* **2008,** *112*, 4748–4752.
7. Szczech, J. R.; Schmitt, A. L.; Bierman, M. J.; Jin, S. Single-Crystal Semiconducting Chromium Disilicide Nanowires Synthesized *via* Chemical Vapor Transport. *Chem. Mater.* **2007,** *19*, 3238–3243.
8. Higgins, J. M.; Schmitt, A. L.; Guzei, I. A.; Jin, S. Higher Manganese Silicide Nanowires of Nowotny Chimney Ladder Phase. *J. Am. Chem. Soc.* **2008,** *130*, 16086–16094.
9. Zhou, F.; Szczech, J.; Pettes, M. T.; Moore, A. L.; Jin, S.; Shi, L. Determination of Transport Properties in Chromium Disilicide Nanowires *via* Combined Thermoelectric and Structural Characterizations. *Nano Lett.* **2007,** *7*, 1649–1654.
10. Lin, Y.; Zhou, S.; Liu, X.; Sheehan, S.; Wang, D. $TiO_2/TiSi_2$ Heterostructures for High-Efficiency Photoelectrochemical H_2O Splitting. *J. Am. Chem. Soc.* **2009,** *131*, 2772–2773.

11. Chou, Y.-C.; Wu, W.-W.; Cheng, S.-L.; Yoo, B.-Y.; Myung, N.; Chen, L. J.; Tu, K. N. *In-Situ* TEM Observation of Repeating Events of Nucleation in Epitaxial Growth of Nano $CoSi_2$ in Nanowires of Si. *Nano Lett.* **2008,** *8*, 2194–2199.
12. Lu, K.-C.; Wu, W.-W.; Wu, H.-W.; Tanner, C. M.; Chang, J. P.; Chen, L. J.; Tu, K. N. *In Situ* Control of Atomic-Scale Si Layer with Huge Strain in the Nanoheterostructure NiSi/Si/NiSi through Point Contact Reaction. *Nano Lett.* **2007,** *7*, 2389–2394.
13. Chueh, Y. L.; Chou, L. J.; Cheng, S. L.; Chen, L. J.; Tsai, C. J.; Hsu, C. M.; Kung, S. C. Synthesis and Characterization of Metallic $TaSi_2$ Nanowires. *Appl. Phys. Lett.* **2005,** *87*, 223113/1–223113/3.
14. Chueh, Y.-L.; Ko, M.-T.; Chou, L.-J.; Chen, L.-J.; Wu, C.-S.; Chen, C.-D. $TaSi_2$ Nanowires: A Potential Field Emitter and Interconnect. *Nano Lett.* **2006,** *6*, 1637–1644.
15. Szczech, J. R.; Jin, S. Epitaxially-Hyperbranched FeSi Nanowires Exhibiting Merohedral Twinning. *J. Mater. Chem.* **2010,** *20*, 1375–1382.
16. Higgins, J. M.; Ding, R.; De Grave, J. P.; Jin, S. Signature of Helimagnetic Ordering in Single-Crystal MnSi Nanowires. *Nano Lett.* **2010,** *10*, 1605–1610.
17. Kang, K.; Kim, C.-J.; Jo, M.-H. Unconventional Roles of Metal Catalysts in Chemical-Vapor Syntheses of Single-Crystalline Nanowires. *J. Appl. Phys.* **2009,** *105*, 122407/1–122407/5.
18. Schmitt, A. L.; Bierman, M. J.; Schmeisser, D.; Himpsel, F. J.; Jin, S. Synthesis and Properties of Single-Crystal FeSi Nanowires. *Nano Lett.* **2006,** *6*, 1617–1621.
19. Schmitt, A. L.; Jin, S. Selective Patterned Growth of Silicide Nanowires without the Use of Metal Catalysts. *Chem. Mater.* **2007,** *19*, 126–128.
20. Schmitt, A. L.; Zhu, L.; Schmeier, D.; Himpsel, F. J.; Jin, S. Metallic Single-Crystal CoSi Nanowires *via* Chemical Vapor Deposition of Single-Source Precursor. *J. Phys. Chem. B* **2006,** *110*, 18142–18146.
21. Xia, Y.; Yang, P.; Sun, Y.; Wu, Y.; Mayers, B.; Gates, B.; Yin, Y.; Kim, F.; Yan, H. One-Dimensional Nanostructures: Synthesis, Characterization, and Applications. *Adv. Mater.* **2003,** *15*, 353–389.
22. Morales, A. M.; Lieber, C. M. A Laser Ablation Method for the Synthesis of Crystalline Semiconductor Nanowires. *Science* **1998,** *279*, 208–211.
23. Morin, S. A.; Bierman, M. J.; Tong, J.; Jin, S. Mechanism and Kinetics of Spontaneous Nanotube Growth Driven by Screw Dislocations. *Science* **2010,** *328*, 476–480.
24. Jin, S.; Bierman, M. J.; Morin, S. A. A New Twist on Nanowire Formation: Screw-Dislocation-Driven Growth of Nanowires and Nanotubes. *J. Phys. Chem. Lett.* **2010,** *1*, 1472–1480.
25. Bierman, M. J.; Lau, Y. K. A.; Kvit, A. V.; Schmitt, A. L.; Jin, S. Dislocation-Driven Nanowire Growth and Eshelby Twist. *Science* **2008,** *320*, 1060–1063.
26. Yang, P. D.; Lieber, C. M. Nanostructured High-Temperature Superconductors: Creation of Strong-Pinning Columnar Defects in Nanorod/Superconductor Composites. *J. Mater. Res.* **1997,** *12*, 2981–2996.
27. Pan, Z. W.; Dai, Z. R.; Wang, Z. L. Nanobelts of Semiconducting Oxides. *Science* **2001,** *291*, 1947–1949.
28. Kang, K.; Kim, S.-K.; Kim, C.-J.; Jo, M.-H. The Role of NiO_x Overlayers on Spontaneous Growth of $NiSi_x$ Nanowires from Ni Seed Layers. *Nano Lett.* **2008,** *8*, 431–436.
29. Sun, Z.-Q.; Whang, S.-J.; Yang, W.-F.; Lee, S.-J. Synthesis of Nickel Mono-Silicide Nanowire by Chemical Vapor Deposition on Nickel Film: Role of Surface Nickel Oxides. *Jpn. J. Appl. Phys.* **2009,** *48*, 04C138/1–04C138/8.
30. Lin, H.-K.; Cheng, H.-A.; Lee, C.-Y.; Chiu, H.-T. Chemical Vapor Deposition of TiSi Nanowires on C54 $TiSi_2$ Thin Film: An Amorphous Titanium Silicide Interlayer Assisted Nanowire Growth. *Chem. Mater.* **2009,** *21*, 5388–5396.
31. Zaitsev, V. K. Thermoelectric Properties of Anisotropic MnSi1.75. In *CRC Handbook of Thermoelectrics*; Rowe, D. M., Ed.; CRC Press: Boca Raton, FL, 1995; pp 299−309.
32. Laurila, T.; Molarius, J. Reactive Phase Formation in Thin Film Metal/Metal and Metal/Silicon Diffusion Couples. *Crit. Rev. Solid State Mater. Sci.* **2003,** *28*, 185–230.
33. Zhang, S. L.; Ostling, M. Metal Silicides in CMOS Technology: Past, Present, and Future Trends. *Crit. Rev. Solid State Mater. Sci.* **2003,** *28*, 1–129.
34. Walser, R. M.; Bene, R. W. First Phase Nucleation in Silicon-Transition-Metal Planar Interfaces. *Appl. Phys. Lett.* **1976,** *28*, 624–625.
35. Pretorius, R. Prediction of Silicide First Phase and Phase Sequence from Heats of Formation. *Mater. Res. Soc. Symp. Proc.* **1984,** *25*, 15–20.
36. Okamoto, H. Fe-Si Phase Diagram (1990 Okamoto H.). In *ASM Alloy Phase Diagrams Center*; Villars, P., Ed.; ASM International: Materials Park, OH, 2010.
37. Zeng, K. J.; Stierman, R.; Chiu, T. C.; Edwards, D.; Ano, K.; Tu, K. N. Kirkendall Void Formation in Eutectic SnPb Solder Joints on Bare Cu and Its Effect on Joint Reliability. *J. Appl. Phys.* **2005,** *97*, 024508/1–024508/8.
38. Fan, H. J.; Gosele, U.; Zacharias, M. Formation of Nanotubes and Hollow Nanoparticles Based on Kirkendall and Diffusion Processes: A Review. *Small* **2007,** *3*, 1660–1671.
39. Salamon, M.; Mehrer, H. Diffusion in the B20-Type Phase FeSi. *Philos. Mag. A* **1999,** *79*, 2137–2155.
40. Walck, S. D.; McCaffrey, J. P. The Small Angle Cleavage Technique: An Update. *Mater. Res. Soc. Symp. Proc.* **1997,** *480*, 149–171.
41. Langford, R. M.; Petford-Long, A. K. Preparation of Transmission Electron Microscopy Cross-Section Specimens Using Focused Ion Beam Milling. *J. Vac. Sci. Technol., A* **2001,** *19*, 2186–2193.
42. Mitchell, D. R. G. DiffTools: Electron Diffraction Software Tools for DigitalMicrograph (TM). *Microsc. Res. Tech.* **2008,** *71*, 588–593.
43. Lensch-Falk, J. L.; Hemesath, E. R.; Perea, D. E.; Lauhon, L. J. Alternative Catalysts for VSS Growth of Silicon and Germanium Nanowires. *J. Mater. Chem.* **2009,** *19*, 849–857.
44. Weill, A. R. Structure of the Eta Phase of the Iron−Silicon System. *Nature* **1943,** *152*, 413.
45. Varadwaj, K. S. K.; Seo, K.; In, J.; Mohanty, P.; Park, J.; Kim, B. Phase-Controlled Growth of Metastable Fe_5Si_3 Nanowires by a Vapor Transport Method. *J. Am. Chem. Soc.* **2007,** *129*, 8594–8599.
46. Yoon, H.; Lee, A. T.; Choi, E.-A.; Seo, K.; Bagkar, N.; Cho, J.; Jo, Y.; Chang, K. J.; Kim, B. Structure-Induced Ferromagnetic Stabilization in Free-Standing Hexagonal $Fe_{1.3}Ge$ Nanowires. *J. Am. Chem. Soc.* **2010,** *132*, 17447–17451.
47. Zhang, S. L.; Smith, U. Self-Aligned Silicides for Ohmic Contacts in Complementary Metal-Oxide-Semiconductor Technology: $TiSi_2$, $CoSi_2$ and NiSi. *J. Vac. Sci. Technol., A* **2004,** *22*, 1361–1370.
48. Gas, P.; d'Heurle, F. M. Kinetics of Formation of TM Silicide Thin Films: Self-Diffusion. In *Properties of Metal Silicides*; Maex, K., Van Rossum, M., Eds.; Institution of Engineering and Technology: 1995; pp 279−292.
49. van Dal, M. J. H.; Huibers, D. G. G. M.; Kodentsov, A. A.; van Loo, F. J. J. Formation of Co−Si Intermetallics in Bulk Diffusion Couples. Part I. Growth Kinetics and Mobilities of Species in the Silicide Phases. *Intermetallics* **2001,** *9*, 409–421.
50. Gas, P.; Thomas, O.; d'Heurle, F. M. Impurity Diffusion in TM Silicide Thin Films. In *Properties of Metal Silicides*; Maex, K., Van Rossum, M., Eds.; Institution of Engineering and Technology: 1995; pp 298−307.
51. Seo, K.; Lee, S.; Yoon, H.; In, J.; Varadwaj, K. S. K.; Jo, Y.; Jung, M.-H.; Kim, J.; Kim, B. Composition-Tuned Co_nSi Nanowires: Location-Selective Simultaneous Growth along Temperature Gradient. *ACS Nano* **2009,** *3*, 1145–1150.
52. Novak, I.; Huang, W.; Luo, L.; Huang, H. H.; Ang, H. G.; Zybill, C. E. UPS Study of Compounds with Metal−Silicon Bonds: $M(CO)_nSiCl_3$ (M = Co, Mn; n = 4, 5) and $Fe(CO)_4(SiCl_3)_2$. *Organometallics* **1997,** *16*, 1567–1572.
53. Manyala, N.; Sidis, Y.; DiTusa, J. F.; Aeppli, G.; Young, D. P.; Fisk, Z. Magnetoresistance from Quantum Interference Effects in Ferromagnets. *Nature* **2000,** *404*, 581–584.